Evaluation of texture parameters for the quantitative description of multimodal nonlinear optical images from atherosclerotic rabbit arteries

Mostaço-Guidolin, Leila B.; Ko, Alex C.-T.; Popescu, Dan P.; Smith, Michael S.D.; Kohlenberg, Elicia K.; Shiomi, Masashi; Major, Arkady; Sowa, Michael G.

Publisher's version / Version de l'éditeur:
https://doi.org/10.1088/0031-9155/56/16/016
Physics in Medicine and Biology, 56, 16, pp. 5319-5333, 2011-07-28

Evaluation of Texture Parameters for the Quantitative Description of Multimodal Nonlinear Optical Images from Atherosclerotic Rabbit Arteries

Leila B Mostaço-Guidolin[1,2], Alex C-T Ko[1,2], Dan P Popescu[1], Michael S D Smith[1], Elicia K Kohlenberg[1], Masashi Shiomi[3], Arkady Major[2], Michael G Sowa[1*]

[1]Institute for Biodiagnostics, National Research Council Canada, Winnipeg, Canada, R3B 1Y6
[2]Dept. Electrical and Computer Engineering, University of Manitoba, E3-559 Engineering Building, Winnipeg, Canada, R3T 5V6
[3]Institute of Experimental Animals, Kobe University, School of Medicine
Kobe 650-0017, Japan

* corresponding author

Abstract

The composition and structure of atherosclerotic lesions can be directly related to the risk they pose to the patient. Multimodal nonlinear optical microscopy provides a powerful means to visualize the major extracellular components of the plaque that critically determine its structure. Textural features extracted from nonlinear optical images were investigated for their utility in providing quantitative descriptors of structural and compositional changes associated with plaque development. Ten texture parameters derived from the image histogram and gray level co-occurrence matrix were examined that highlight specific structural and compositional motifs that distinguish early and late stage plaques. Tonal-texture parameters could be linked to key histological features that characterize vulnerable plaque: the thickness and density of the fibrous cap, size of the atheroma, and the level of inflammation indicated through lipid deposition. Tonal and texture parameters from nonlinear optical images provide objective metrics that correspond to structural and biochemical changes that occur within the vessel wall in early and late stage atherosclerosis.

1. Introduction

Arterial diseases, especially atherosclerosis, are leading contributors to morbidity and mortality in Western societies, and these diseases are also on the rise globally [1,2]. There is a need for new tools to better investigate the underlying mechanisms of atherosclerosis and characterize the various stages of atherosclerosis progression. Nonlinear optical (NLO) microscopy, a primarily label-free method, is a useful tool for studying key facets of atherosclerosis. Its label-free characteristic combined with high sensitivity and specificity for major extracellular molecules makes it an attractive alternative to conventional histology or fluorescence microscopy in studying arterial structures and vessel wall composition. The optical sectioning capability of NLO methods also provides a means of imaging bulk tissue in 3-D. Three NLO methods were employed in this study. Two-photon excited autofluorescence (TPEF) has the capability to specifically image extracellular elastin fibers, while second harmonic

generation (SHG) can probe type-1 collagen fibrils. Coherent anti-Stokes Raman scattering (CARS), when tuned to image the C-H stretching vibrations, can quickly visualize lipid-rich structures, intracellular and extracellular lipid droplets in unstained intact tissue. It is already known that both elastin and collagen are the major structural proteins implicated in the remodeling of the arterial wall during plaque development while lipid accumulation is a hallmark feature of atherosclerosis. Therefore, NLO methods are particularly suited to understanding the role and interplay between these key extracellular molecules involved in plaque development. Several studies have demonstrated the use of NLO microscopy to image arterial tissue [3-8]. However, few of these studies have provided quantitative descriptors of the images and related these metrics to the development of atherosclerosis or vascular wall anatomy and pathology. In this paper we explore the utility of using tonal and texture features from nonlinear optical images in correspondence to the structural and biochemical changes that occur within the vessel wall in early and late stage atherosclerosis. The aim of this work is to validate a series of texture metrics as objective methods for quantification of NLO images acquired from samples with vascular wall pathology related to atherosclerotic plaque development.

2. Experimental Materials and Methods

2.1. Animal model and tissue preparation

This study was approved by the local animal care committee at the Institute for Biodiagnostics, National Research Council Canada. In this study, myocardial infarction prone Watanabe heritable hyperlipidemic rabbits, designated as WHHLMI rabbits [9,10], were used as an animal model to mimic spontaneous myocardial infarction in humans. Due to a hereditary defect in LDL (low density lipoprotein) processing, WHHLMI rabbits develop atherosclerotic plaques without requiring a modified diet. Arterial samples harvested from six WHHLMI rabbits aged 4, 10, 18 and 24 months were studied. This sampling represents stages of atherosclerotic disease progression, with the 24 months-old rabbit being considered to be nearing the end of its life cycle.

During harvest, segments of tissue starting from the ascending aorta to the external iliac artery were excised from all specimens and then rinsed in heparinized saline. The exterior surfaces of these aorta sections were delicately cleaned of connective tissue prior to being subdivided into ~20-30 mm-long sections, process resulting in 7 tissue pieces from each of the six WHHLMI rabbits. Additionally, matched short segments were set aside for histology. Each section was cut open longitudinally exposing the luminal surface. The samples were placed in petri-dishes with the luminal surface facing up on a moist surface and hydration was maintained throughout the measurements by periodically applying phosphate buffered saline (PBS) solution. Digital photos of the luminal surface were acquired and regions of interest were identified prior to measurements.

2.2. Histological images

For histology, the artery was cross-sectioned on a cryotome into sections while embedded in Optical Cutting Temperature medium. The tissue sections prepared for NLO imaging received no further treatment after cutting while those prepared for histology were immersion-fixed in either 95% ethanol or 10% buffered formalin based on individual staining protocols. Artery sections used in multimodal NLO imaging were compared to adjacent H&E (hematoxylin and eosin) stained sections which revealed

general tissue morphology, picro-sirius red stained sections highlighting collagen and elastin fibers under cross-handed circularly-polarized condition [11], and oil red O staining accenting high-lipid structures . Histology images were obtained using a 10x air objective lens on a Zeiss Axio Observer Z1 system equipped with AxioCam ICc3 CCD camera (Carl Zeiss Canada, Toronto, ON, Canada).

2.3. Multimodal NLO microscopic imaging

A home-built multimodal nonlinear optical (NLO) laser scanning microscope was used for two-photon excited fluorescence (TPEF), second harmonic generation (SHG) and coherent anti-Stokes Raman scattering (CARS) imaging of arterial tissue. While most bulk-tissue imaging was accomplished using backscattered (epi-) configuration as illustrated in Figure 1, alternative forward-CARS and forward-SHG configuration was used to image thin-sections of arterial vessel. Technical details of this NLO laser scanning microscope were previously reported [8,12] and also shown in Figure 1. In summary, this is a photonic-crystal fibre (PCF) based femtosecond CARS microscope powered by a femtosecond Ti:Sapphire oscillator (Tsunami, Spectra-Physics) with operating wavelength centered at 800nm. The PCF was pumped by the 800nm femtosecond pulses and a broadband emission was generated. The near-IR portion of this broadband emission was selected to act as the Stokes beam. In the current setup, the frequency difference between the pump and the Stokes beams was tuned to match the vibrational frequency of the C-H stretching mode for fast lipid imaging. This system is equipped with three non-descanned PMT detectors for capturing co-localized TPEF, SHG and CARS signals simultaneously through an array of optical filters and dichroic mirrors. As evaluated in previous studies [13-15], the PMT detectors used in this study present low cross-talk and fast response times. We used a 20×, 0.75-NA objective lens (Olympus) in order to combine a large field of view and a good spatial resolution. Typical laser powers used for imaging were measured at 25mW and at 8mW for the pump beam and the Stokes beam, respectively. We used the Scanimage software (version 3.5) for hardware control and image acquisition [16]. Corrections for illumination variations, dark current and signal intensity normalization were carried out according to the procedure outlined previously [17,18].

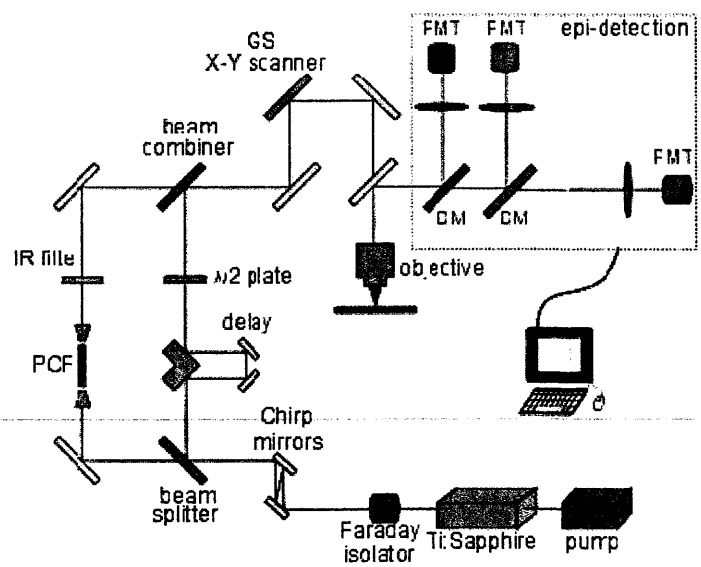

Figure 1 - Schematic of the home-built multimodal nonlinear optical laser scanning microscope. Light source for TPEF and SHG imaging is a Ti:Sapphire femto-second oscillator (Tsunami,Spectra-Physics). For CARS imaging, Stokes pulses are generated in PCF which is pumped by the same Ti:sapphire laser. F-ISO: Faraday isolator; CM: chirp laser mirrors; BS: beam splitter; NIR-F: near-IR filter; GS: galvo scanner; DM: dichroic mirror; OBJ: objective lens; BF: bandpass filter; NDF: neutral density filter; λ/2: half waveplate.

2.4. Image texture analysis

Ten texture parameters were determined using the histogram or gray level co-occurrence matrix (GLCM) of the image. The "co-occurrence matrix" represents the probability of occurrence of a pixel pair, with a given graytone difference, separated by predefined distance taken in a predefined direction while the image "histogram" is the frequency of occurrence of a gray tone in an investigated region.

Image first-order statistics are not textural features because only the intensities of individual pixels is considered independently from their neighboring pixels. These first-order statistics merely describe the gray levels of the histogram corresponding to an image. Five first order parameters, the mean, standard deviation, integrated density, skewness, and kurtosis, extracted from the histogram of our images proved to be useful. The mathematical expressions describing these parameters [19] are presented in Table I. The mean and integrated density provide measures of the overall lightness/darkness of the image, while the standard deviation describes its overall contrast. The skewness quantitatively evaluates the asymmetry of the shape of the distribution of pixel intensities while the kurtosis measures the *peakedness* of the distribution relative to the length and size of its tails.

Image second order statistics depend on the spatial arrangement of the gray levels present in the region of interest and provide textural information for that region. Co-occurrence matrices describe the second order statistics of the images. This method is based on the estimation of the second order joint conditional probability density functions $P_{d,\theta}(i,j)$. Each $P_{d,\theta}(i,j)$ is the probability of going from a grey level i to a gray level j in a given direction θ at a given intersample spacing d. The co-occurrence matrix $P_{d,\theta}(i,j)$ is a representation of the estimated values. It is a square matrix of dimension N_g (N_g is the number of gray levels in the image). To summarize the content of a co-occurrence matrix, a number of texture features can be defined. A set of 14 features, defined by Haralick *et. al.* [19], were studied for their value in relating multimodal NLO images to vessel wall morphology. These were the angular second moment, inertia, correlation, variance, inverse difference moment, sum average, sum variance, difference variance, sum entropy, entropy, difference entropy, information measures of correlation one, information measures of correlation two, and maximum probability. However, only 5 of them were found to be useful in the context of characterizing structures in the NLO images of the vessel wall. Only the results using the energy, inertia, correlation, inverse difference moment, and entropy texture features are reported. The mathematical expressions defining these texture features are given in Table I.

Table I – Texture features and its mathematical expressions.

Textural feature category	Feature	Expression	Interpretation
FOS	Mean	$\mu = \sum_{i=0}^{N-1} i \sum_{j=0}^{N-1} P_{i,j} = \sum_{j=0}^{N-1} j \sum_{i=0}^{N-1} P_{i,j}$	average gray value

FOS	Standard deviation	$\sigma=\sum_{i=0}^{N-1}(i-\mu)^2\sum_{j=0}^{N-1}P_{i,j}$	standard deviation of the gray values used to generate the mean gray value
FOS	Integrated density	$I=\sum_{i=0}^{N-1}n(i)i$	product of image's area and mean gray value
FOS	Skewness	$\mu_3=\sigma^{-3}\sum_{i=0}^{N-1}(i-\mu)^3P_i$	third order moment about the mean. It quantifies how symmetrical the distribution is
FOS	Kurtosis	$\mu_4=\sigma^{-4}\sum_{i=0}^{N-1}(i-\mu)^4P_i-3$	fourth order moment about the mean. It quantifies whether the shape of the data distribution matches the Gaussian distribution
GLCM	Energy	$\sum_{i,j=0}^{N-1}P_{i,j}^2$	degree of image's texture directions according to the perception of human eyes (also called uniformity)
GLCM	Correlation	$-\sum_{i,j=0}^{N-1}P_{i,j}\left[\frac{(i-\mu_x)(j-\mu_y)}{\sigma^2}\right]$	linear dependency of grey levels on those of neighbouring pixels.
GLCM	Inertia	$\sum_{i,j=0}^{N-1}(i-j)^2P_{i,j}$	representation of pixels entirely similar to their neighbour,
GLCM	Inverse Difference Moment	$\sum_{i,j=0}^{N-1}\frac{P_{i,j}^2}{1+(i-j)^2}$	measure of the amount of local uniformity present in the image (also called homogeneity)
GLCM	Entropy	$-\sum_{i,j=0}^{N-1}P_{i,j}\log P_{i,j}$	measure of randomness

FOS: first order statistics; GLCM: gray level co-occurrence matrix; P: probability density function;

The co-occurrence matrix was calculated in four orientations: horizontal, vertical, and the two diagonals (directions defined by four angles: 0°, 45°, 90°, and 135°), and the average value obtained by considering the four directions was considered. A window size with 8 pixels was adopted to extract features from 16bit images. The post image processing was performed in ImageJ ver1.42b. Image background correction, intensity normalization and calculation of various image texture parameters were carried out using Matlab7.5. A custom-built texture analysis toolkit based on some of the texture analysis functions available in the MATLAB image processing toolbox was used to calculate GLCM parameters. FOS parameters were calculated by using ImageJ's histogram analysis toolbox [20].

3. Results and Discussion

The composition and structure of atherosclerotic lesions are critical determinants of the risk they pose to the patient. Modalities capable of characterizing the atherosclerotic lesion may be helpful in understanding its natural history and in detecting lesions with a high risk for acute events. Generally, three histological features of plaque have been taken into account as closely correlated with the risk of an acute event: size of the atheroma or plaque, thickness of the fibrous cap that covers the lipid rich necrotic core of the plaque, and inflammation [21]. Current diagnostic imaging techniques aid in the visualization of plaque and arterial narrowing. However, most of these diagnostic modalities detect only one of the histological features that define the vulnerability of the plaque to rupture or fibrous cap erosion. NLO microscopy can be used to visualize the major features that define plaque vulnerability, histologically. Through texture analysis of multimodal NLO images it is possible to extract and quantify these features, which can be associated with plaque development, providing a turn-key method to analyze NLO images of the vessel wall and relating them to vessel wall pathology.

3.1. Anatomical and Biochemical Validation

NLO images of sections and bulk tissue of the aorta vessel were characterized through a visual comparison with histological images from matched sections as well as anatomical images from optical coherence tomography (OCT), as shown in Figure 2. Four different types of histological stains were compared with the multimodal NLO images of the adjacent unstained artery section (shown Figure 2B). OCT image is shown Figure 2A. Figures 2C, 2D, 2E and 2F illustrate H&E (bright field), oil red O (bright field) and picro-sirius red (circularly polarized light) and Verhoeff's stains of adjacent artery sections, respectively, to help visualize general tissue morphology and particular extra-cellular components. These stains highlight elastin fibers (Figure 2F), collagen fibers (Figure 2E), and lipid deposits (Figure 2D). However, the accumulation and localization of each compound can also be observed in the corresponding multimodal NLO image, without using stains. Three major biochemical components relevant to atherosclerotic plaque development were observed in the merged RGB images generated by the multi-modal NLO microscopy measurements, where elastin fiber is the predominant feature in the TPEF channel that is color-coded in green, the blue color-coded SHG channel highlights collagen fibrils while the CARS channel (red) shows lipids. Extra-cellular elastin is observed in the tunica media while collagen fibrils are observed in tunica adventitia, at the intima-media boundary and as a component forming the cap on the atherosclerotic plaque. Meanwhile, the lipid formations within the plaque bodies that are detected by the CARS component of the multimodal image are also observed in the matched oil red O stained sections.

OCT, an anatomical imaging technique where contrast is based on differences of refractive index within the tissue, was used to further validate the features observed in multimodal NLO microscopy. Several samples measured by NLO microscopy and analyzed by histology were compared to matched measurements made with swept-source Fourier-domain optical coherence tomography (OCT). A 3x3 Mach-Zehnder quadrature interferometer configuration with a swept-source, with a measured sensitivity of 107 dB, which has been described elsewhere [22, 23] was used for these OCT measurements. Based on differences in the gray values observed within the OCT images (an example is shown in Figure 2A), it is possible to distinguish different features of the atherosclerotic lesion [24-27]. The diffuse intimal thickening appears as the uppermost reflective layer, bound by a high reflective internal elastic lamina. In the OCT image, the media of the vessel wall appears as a uniform weak back scattering layer underneath the highly backscattering internal elastic lamina. Lipid rich areas and calcifications observed in the

histology and NLO images could be matched to regions with a lower backscattered signal in the OCT images. There were two parameters used in order to establish correlations between the tissue morphology and the characteristics of OCT images: i) the OCT signal attenuation as it propagates within the sample and ii) box-counting-based fractal analysis applied to the intensity patterns displayed in OCT images. Both methods were very effective at identifying the various layers of healthy coronary arteries [25] but were less sensitive in resolving pathological features in the arteries of WHHLMI rabbits [28]. NLO imaging is able to provide more details about the structural and chemical features of the vessel wall due to the particular biochemical specificity of each of the independent imaging channels compared to OCT imaging which relies only on light scattering for image contrast.

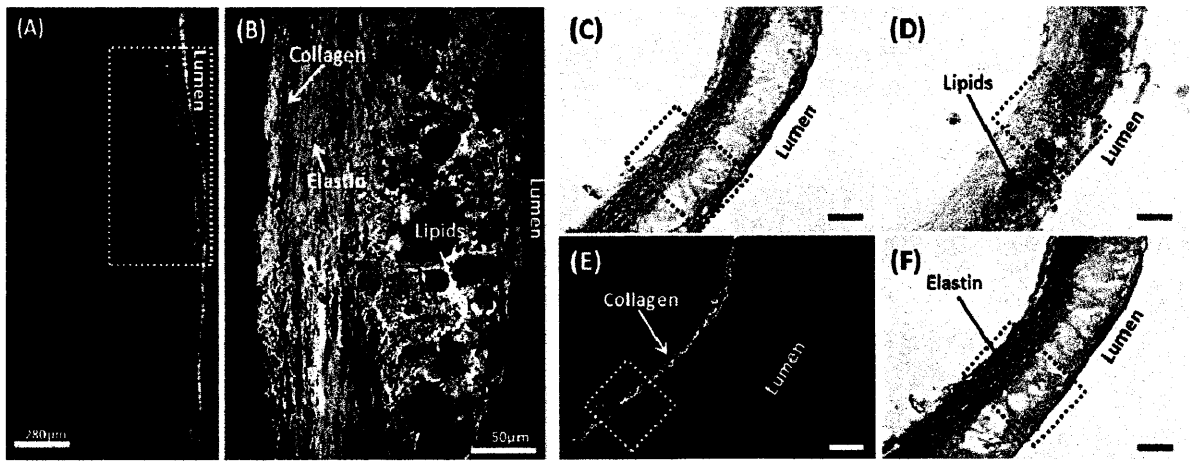

Figure 2 – Atherosclerotic plaque features and its major components visualized by (A) OCT image; (B) NLO microscopy, where the elastin fiber is color-coded in green (TPEF), collagen fibrils in blue (SHG) and lipids in red (CARS). Both SHG and CARS signals are collected in the forward-direction while TPEF is collected in the backscattered (epi-)direction; and histological images of adjacent artery sections stained with (C) H&E (bright field), (D) oil red O (bright field). The section in (E) and (F) is double stained with picro-sirius red (collagen) and Verhoeff's (elastin). (E) was imaged using circular polarized light to detect the collagen fiber stained by picro-sirues red and, in (F) the bright field image captures the elastin fibers stained black by the Verhoeff's.

The correspondence between the histological sections, OCT anatomical images, and the multimodal NLO images validates our understanding of what gives rise to contrast in the multimodal NLO images of the vessel wall.

3.2. Evaluation of Plaque Depth

Atherosclerotic lesions develop progressively through a series of events leading to the development of mature lesions named *atheromatous plaques*. Figure 3A is a sketch representing a mature lesion consisting of a fibrous cap (I), composed largely of smooth muscle cells (SMC), which produce collagen, small amounts of elastin, and glycosaminogycans; (II) a necrotic core, composed mainly of lipid-filled macrophages and necrotic smooth muscle cells debris; and (III) the media layer, consisting mainly of smooth muscle cells.

Figure 3B compares a sequence of NLO images acquired from arterial samples, with the lumen exposed to the incoming probe beam. An image is obtained by scanning the focus of probe beam across a plane located at a particular depth within the sample. By changing the focal plane, images were acquired at different depths into the artery. The first set of images is an example of the optical sectioning obtained by recording the TPEF, SHG and CARS intensities at various depths within the aorta of a 4 month old rabbit. This set of images represents an early lesion. The second set shows the optical sectioning of an older plaque, a specimen obtained from a 24 month old rabbit. These optical sections generated from integrating the multimodal NLO images resolve many of the classic histological features associated with plaque development and provide the depth dependence of these features.

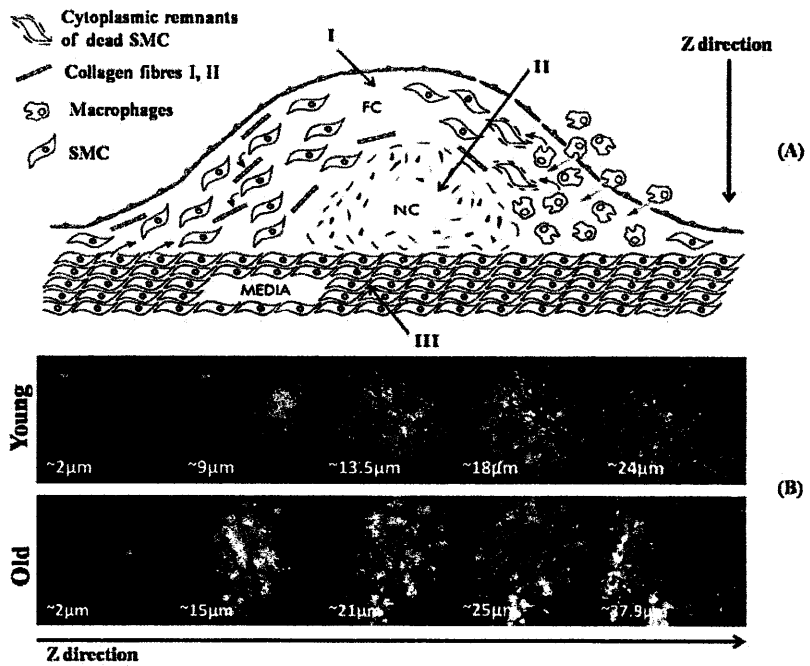

Figure 3 – (A) The atherosclerotic plaque is composed of three major layers: (I) fibrous cap (FC), consists mainly of smooth muscle cells (SMC), which produce collagen, small amounts of elastin, and glycosaminogycans; (II) necrotic core (NC) consisting of lipid-filled macrophages, necrotic smooth muscle and cellular debris; and (III) the media layer, consisting of smooth muscle cells **(B)** Examples of multimodal NLO images acquired with a 20x air lens at various depths within atheromatous plaques. The first image set shows plaque from a 4 month old rabbit, while the second image set is from the aorta harvested from a 24-month old rabbit. Blue: SHG (collagen fibrils). Red: CARS (lipids). Green: TPEF (fluorescent macromolecules).

3.3. Texture Analysis

Five first order statistical parameters (mean, standard deviation, integrated density, kurtosis, and skewness) were calculated for the images acquired from each NLO channel. A number of these features were sensitive to the changes occurring in the vessel wall related to plaque development. Approximately 90 measurements were performed along the aorta extracted from the 3 oldest rabbits, while 60 different points were measured for the three specimens in the younger group. The same incident power of 25/8mW was maintained. The mean value for each group (young and old) and its standard deviation were

calculated for each calculated texture feature. A table is available as supplementary material, to illustrate an example on how each NLO image channel relates to the variation of its respective texture parameters.

Comparing values of the mean gray level and its standard deviation, it is possible to verify significant changes occurring to the SHG signal as deeper regions of the samples are probed, as shown in Figure 4A and 4B. In these figures, the reading on x-axis represents the position of the imaging focal point in relation to the lumen surface. In a healthy artery, the collagen fibers are mostly located within the tunica media, delimited by an internal elastic membrane [12]. In contrast, in diseased arteries, common among the older specimens, collagen fibers are found to extend beyond an interrupted internal elastic layer [12,17]. Plaques observed in old animals present a mean gray level value around 4 times more intense than ones associated with plaques in younger animals. This difference reflects the general feature that fibrous caps of plaques from old animals are denser than the caps observed in young animals. These histological characteristics of atherosclerosis correlate with our experimental measurements where higher SHG intensities are observed at depths between 15-30μm in the samples coming from the older specimens, whereas the maximum SHG intensities are observed at depths of around 5μm in samples harvested from younger animals.

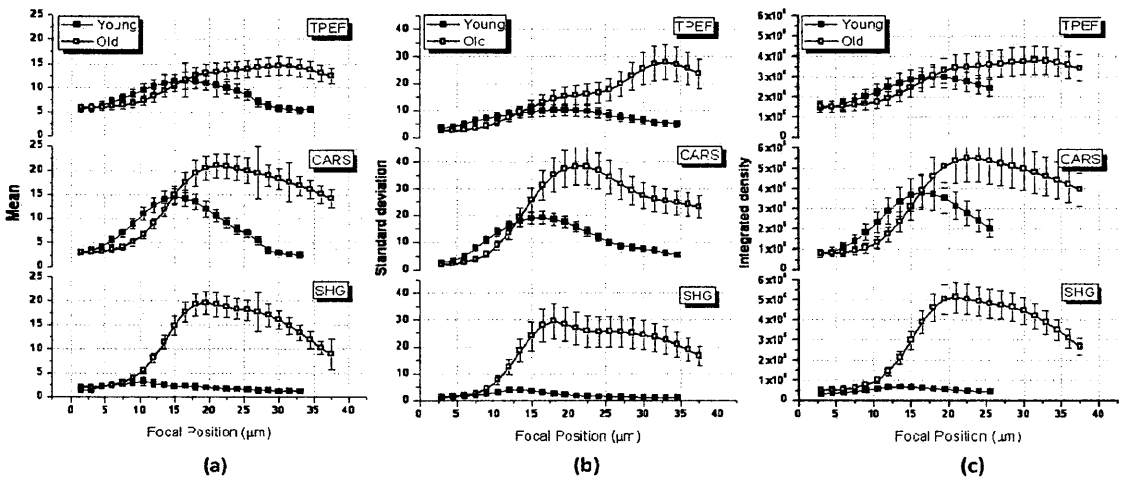

Figure 4 – First order statistics: **(A)** mean, **(B)** standard deviation and **(C)** integrated density. Features were individually calculated for each NLO mode (TPEF, CARS, and SHG) and analyzed as a function of imaging depth within the aorta wall. In most cases, distinct differences were observed in the first order statistics between young and old animals and with imaging depth. The analysis is done starting from the sample surface (i.e., the lumen) to depths of almost 40μm. The intensity recorded for each of the NLO channels depends on both depth and specimen age. The old group includes specimens that were 18 and 24-months old while the young group contains specimens that were from animals that were 4 and 10 months old.

Observing the variation of the CARS signal, its maximum intensity in older animals appeared approximately 10μm deeper than observed in young animals. Consistent with histology, the CARS signal, which highlights lipids, shows that lipid accumulation occurs in the intermediate portion of the plaque. For example, in the case of young animals, the lipid pool appears approximately 5μm deeper than collagen fibrils signaled by the SHG channel and associated with fibrous cap formation over the surface of lipid pools. Proliferation of collagen fibrils and lipid accumulation play key roles in the development and vulnerability of atherosclerotic plaques where a thin fibrous cap coupled with a large lipid filled core

represent a high risk lesion. Old animals present a more complex necrotic core, due to extended lipid pools and a higher concentration of both collagen fibrils and lipid-rich cells in the same region, near the arterial lumen [29]. In fact, the strongest CARS and SHG signals are observed to be almost overlapped in the plaques from older animals. On the other hand, the maximum CARS and SHG signals are observed at different depths for the less fully developed plaques in the young specimens.

A significant TPEF signal starts at depths of about 10μm and extend throughout the rest of the optical section of the plaque. The origin of the TPEF could be either from elastin fibers or several types of macromolecules associated with plaque formation. It is not trivial to establish what generates the TPEF without histological correlation. We observe fluorescent objects within fibrous caps and lipid cores whose origin has not yet been determined. The TPEF signal that we observed clustering in small groups among the collagen fibers [12,29,30], have been identified as foam cells (macrophages with intracellular lipid droplets). As the lipid core is mainly necrotic cells, and the fluorescent objects appear as different sizes, the corresponding TPEF signal could be also related to extracellular lipid droplets.

A study conducted by Blankenhorn *et al.* [31] has reported a strong, green, one-photon auto-fluorescence generated from the lipid core of atherosclerotic plaques. This has been associated with carotenoids, which are known to be lipophilic. Another study found one-photon auto fluorescence from various biochemical components, which are known to be present in atherosclerotic plaques (e.g., oxidized lipoproteins and cholesterol esters). Further studies have been supporting the hypothesis that the TPEF signal is related to lipid-rich substances in the plaques [32].

The kurtosis and the skewness of the gray level intensity histograms were calculated and the results were shown in Figure 5. The skewness value is a first order texture feature that measures the extent to which the pixel intensity values are not distributed in a Gaussian manner. In other words, the skewness of a set of luminance values indicates the imbalance between extents of areas (or number of pixels) that are darker or lighter than the mean. On the other hand, even-order statistics (e.g. variance and kurtosis) are always the same for an image and its negative, so that they are blind to any asymmetries in light and dark (such as those that occur with highlights and shadows) [33]. The kurtosis is a measure of the spread of gray tones about the mean.

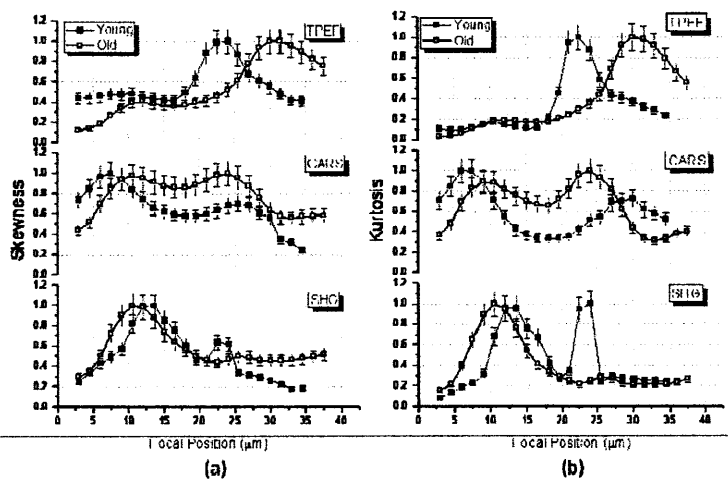

Figure 5 –First order statistics: (A) skewness and (B) kurtosis. Features were individually calculated for each NLO mode (TPEF, CARS, and SHG) and were analyzed as a function of depth and specimen age, where the old and young group corresponds to specimens 18 and 24-month old, and 4 and 10-month old, respectively.

According to data presented in Figure 5, due to the formation of fibrous caps, the SHG signal from old rabbits presents an asymmetrical pattern more superficially localized than the SHG pattern observed in plaques of younger animals. The maximum value of asymmetry is located approximately 4μm deeper in young animals than in old specimens.

The CARS images show a bimodal variation in skewness and kurtosis as a function of depth into the vessel wall. In the more fully developed plaques, high values of skewness and kurtosis extend deeper into the wall of the aorta (approx. from 10μm to 25μm). Considering that the CARS signal is associated with lipid deposits and that old plaques characteristically have deeper and more extensive accumulation of lipids than plaques in young animals, the skewness and kurtosis measures are consistent with the lipid profiles observed in these plaques.

The TPEF fluorescence images show similar depth dependence for both texture features. Young plaques present a maximum in skewness and kurtosis at around 20-25μm below the surface; on the other hand, the maximum of these parameters for old plaques occur around 25-35μm below the surface. Glossy structures in the images can be observed 10μm shallower in young plaques compared to old ones.

Five texture parameters extracted from the co-occurrence gray level matrix (GLCM) were selected from the 14 defined by Haralick *et al.* [19]: inverse difference moment (IDM), energy, inertia, entropy, and correlation. In Figure 6, data related with IDM, energy and contrast are presented. Considering that the IDM (also called local homogeneity) quantifies the local similarities inside the computational window, it is expected to be larger for GLCMs with elements concentrated near the diagonal. These GLCMs correspond to textures of organized and poorly contrasted features, with only a few gray levels at the same distance d from one another. This parameter quantifies the degree of homogeneity in the region of interest.

Associated with the CARS signal, we observe that lipid accumulation in older plaques is more homogeneous than in the plaques of young animals (Figure 6A). At approximately 25μm into the wall of the aorta, it is possible to note that fluorescent structures (TPEF channel) detected in old plaques tend to be more homogeneous than those identified in young plaques. However, this texture feature for the collagen fibril distribution (SHG channel) showed no significant statistical difference between young and old plaques.

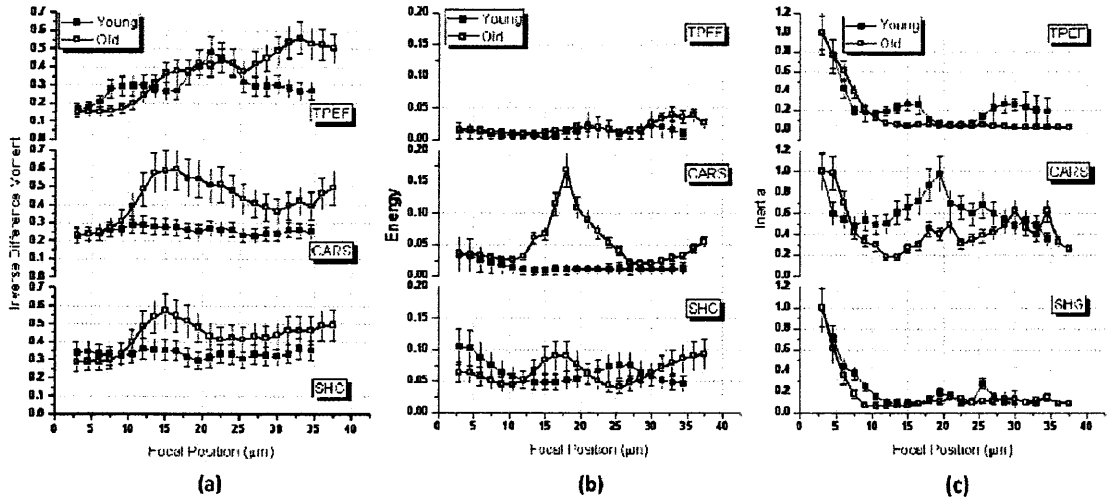

Figure 6 – Second order parameters extracted from the GLCM: (A) Inverse difference moment (IDM); (B) Energy; (C) Inertia. Features were individually calculated for each NLO mode (TPEF, CARS, and SHG).

The energy feature, shown in Figure 6B, is sometimes referred to as the second angular moment or uniformity of the GLCM. The lowest value of energy is attained when all the $P_{d,\theta}(i,j)$ are equal, and there are no dominant gray levels. Most gray levels are equally probable. The energy parameter associated with the TPEF channel has a constant and low value over the depth of the optical scan; energy values for the SHG channel show some variations, but they are not statistically significant. On the other hand, the energy parameter calculated for the CARS images shows a distinctly different depth profile between the younger and older plaques. The high energy values observed in the CARS signal from older plaques at a depth centered around 18μm shows that only a few gray levels dominate the image at this depth. The region inside the computational window is more homogeneous or exhibits some regular structures. In this case, regular structures are concentrated only at the region between depths of 10 and 30μm from the surface of the plaque developed by old animals. Through this texture parameter, it is possible to locate and approximately estimate the size of the lipid core. The depth and size of the lipid core are important histological features of a plaque where the amount of thrombogenic (lipid) material is related to its potential to cause a significant ischemic event.

The inertia texture feature, presented in Figure 6C (also called second difference moment), is very sensitive to large differences occurring inside the co-occurrence matrix. Highly contrasted regions will have a high inertia, whereas more homogeneous regions will have a low inertia. Information acquired from SHG and TPEF present similar contrast level in both old and young plaques. Meanwhile the inertia from the CARS signal shows some fluctuation concentrated at the intermediate portion of the plaque (around 10 and 30μm). It can be related to the lipid accumulation inside the necrotic core, being more homogeneous in the plaques developed by old animals.

Observing the images presented in Figure 7, it is possible to note several morphological differences among plaques developed by young and old animals. The fibril cap features collagen formed in thick bundles organized in a non-directional structure, as showed by the SHG-generated images in Figure 7A. The collagen assembly is significantly thicker in the plaque caps developed in older animals compared to the formations observed in young rabbits. Besides these changes in collagen, we observe that

lipid accumulation starts as droplets, becoming bigger (as shown in Figure 2) and being more homogeneously distributed in the tissue (Figure 7B) with specimen age. Finally, the images on the TPEF channel show small, round, fluorescent objects of various sizes that can be seen clustered in the spaces between the collagen fibers in young plaques as in Figure 7C. Their distribution follows the same pattern observed in the CARS images: in old plaques fluorescent objects are homogeneously distributed in the tissue as compared to the distribution observed in young plaques, which is much sparser.

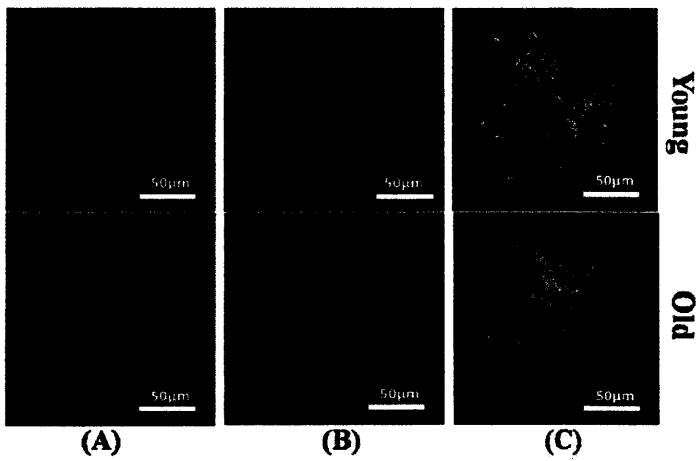

Figure 7 – Images from three NLO channels using a 20x air lens. Each NLO channel is shown separately (at a focal position around 25-30μm below the sample surface for the old specimen, and around 10-20μm below the sample surface for the young specimen). (A) Blue: SHG (collagen fibrils); (B) red: CARS (lipids); (C) Green: TPEF (fluorescent macromolecules). Images for the early plaque were acquired from a sample harvested from a 4-month old WHHLMI rabbit and images of the developed plaque were acquired from a sample collected from an 18-month old WHHLMI rabbit.

The textural parameters provide a means of capturing and quantifying the morphological changes that are observed in these images. Additional information can be acquired by analyzing the entropy and the correlation of NLO images. The correlation quantifies the dependence of gray levels between two pixels separated by distance *d*. Low correlation means that the gray levels are generally independent from one another, i.e., there is no regular structure in the image. However, if correlation is high, there is a high probability that one or several patterns repeat themselves inside the computational window. The entropy measures the lack of spatial organization inside the computational window. Entropy is high when all $P_{d,\theta}(i,j)$ are equal, which corresponds to a rough texture, and low when the texture is more homogeneous or smoother. As discussed previously, old plaques have a denser collagen network than young plaques. On the other hand, collagen fibers in young plaques tend to be spatially more randomly distributed compared to the collagen network observed in older plaques. Therefore, this denser and more homogeneous distributed collagen network in older plaques (Figure 2B and Figure 7A) can be quantified by the entropy and correlation of the SHG images, as shown in Figure 8.

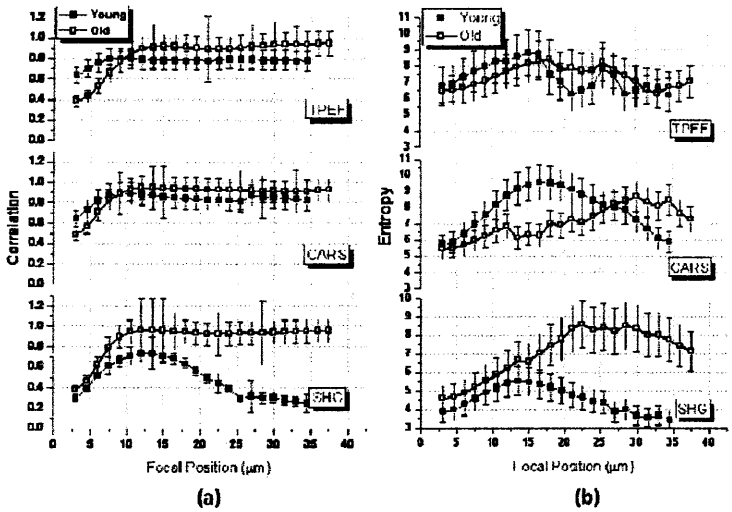

Figure 8 – Second order parameters extracted from the GLCM: (A) correlation and (B) entropy. Features were individually calculated for each NLO mode (TPEF, CARS, and SHG), being analyzed as function of plaque depth.

The entropy of the CARS images could also be useful for tracking the randomness of lipid accumulation in young plaques. Entropy values from CARS images increase with depth in young rabbits and they are consistent with the observation that older, more developed, plaques tend to have larger lipid pools filled by homogeneously distributed lipid structures, therefore presenting lower entropy values.

It is also worth noting that variations in some texture parameters at different locations along the longitudinal axes within the aorta were observed. For instance, some GLCM features of the SHG channel show differentiating power between locations experiencing turbulent blood flow (e.g. arterial arch) and laminar blood flow (e.g. external iliac artery) along the aorta. We believe that such observation could lead to a useful functionality of the NLO technique to aid in interpreting underlying effect of blood flow on plaque's growth. More study is needed in order to fully interpret the data.

4. Conclusions

Atherosclerotic plaques and plaque development are complex systems where the composition and structure vary greatly with respect to age, the location along and within the vessel. Multimodal NLO microscopy is a powerful technique that can be used to visualize the extracellular components, collagen, elastin, and lipids; all of which are major biochemical constituents implicated in plaque development. Determining the spatial distribution of these plaque components rapidly and in a manner that is consistent with conventional microscopy makes NLO microscopy a potential adjunct to routine histopathology. The attractive feature of NLO microscopy is the ability to use optical sectioning to examine bulk tissue without the need for sectioning and staining the tissue. To extend NLO microscopy beyond a qualitative tool for visualization, we investigated the use of textural analysis of the images to provide objective measures of plaque pathology. A set of textural parameters extracted from NLO images provided quantitative descriptors that could be linked to specific structural and compositional motifs that characterize early and late stage plaques. Image histogram and gray level co-occurrence matrix (GLCM) were used to quantitatively evaluate TPEF, SHG and CARS images in relation to three main histological

features that characterize vulnerable plaque: the thickness of the fibrous cap, size of the atheroma, and lipid deposition as related to the level of inflammation. Changes in collagen fiber orientation and lipid accumulation into the aorta wall, and changes in their spatial distribution and patterning could also be quantified by textural features. Most notably, many of the first and second order tonal-texture parameters showed distinctly different depth profiles between the images from young and older specimens that can be rationalized in terms of the differences in the composition and structure of the lesions along their development path. Our results show that tonal-texture parameters offer objective and useful metrics to quantify vessel wall pathology associated with plaque development.

5. References

1. Libby P 2006 Atherosclerosis: disease biology affecting the coronary vasculature *Am. J. Cardiol.* **98** S3–9
2. Hansson G K 2005 Inflammation, atherosclerosis, and coronary artery disease *N. Engl. J. Med.* **352** 1685– 95
3. Le T T, Langohr I M, Locker M J, Sturek M, Cheng J-X 2007 Label-free molecular imaging of atherosclerotic lesions using multimodal nonlinear optical microscopy, *J. Biomed. Opt.*,**12(5)**, 054007
4. Zoumi A, Lu X, Kassab G S, Tromberg B J 2004 Imaging Coronary Artery Microstructure Using Second-Harmonic and Two-Photon Fluorescence Microscopy, *Biophysical J.* **87**, 2778-2786
5. Wang H-W, Langohr I M, Sturek M, Cheng J-X 2009 Imaging and quantitative analysis of atherosclerotic lesions by CARS-based multimodal nonlinear optical microscopy, *Arterio. Thromb. Vasc. Biol.*, **29**, 1342-1348
6 Lim R S, Kratzer A, Barry N P, Miyazaki-Anzai S, Miyazaki M, Mantulin W W, Levi M, Potma E O, Tromberg B J 2010 Multimodal CARS microscopy determination of the impact of diet on macrophage infiltration and lipid accumulation on plaque formation in ApoE-deficient mice, *J. Lipid Res.* **51(7)**, 1729-37
7. Kim S H, Lee E S, Lee J Y, Lee E S, Lee B S, Park J E, Moon D W 2010 Multiplex coherent anti-stokes Raman spectroscopy images intact atheromatous lesions and concomitantly identifies distinct chemical profiles of atherosclerotic lipids, *Circ Res.* **106(8),** 1332-41
8. Ko A C-T, Ridsdale A, Smith M S D, Mostaço-Guidolin L B, Hewko M D, Pegoraro A F, Kohlenberg E K, Schattka B, Shiomi M, Stolow A and Sowa M G 2010 Multimodal nonlinear optical imaging of atherosclerotic plaque development in myocardial infarction-prone rabbits *J. Biomed. Opt.* **15** 020501
9. Shiomi M, Ito T, Yamada S, Kawashima S and Fan J 2003 Development of an animal model for spontaneous myocardial infarction (WHHLMI rabbit) *Arterioscler. Thromb. Vasc. Biol.* **23** 1239–44
10. Shiomi M, Ito T, Yamada S, Kawashima S and Fan J 2004 Correlation of vulnerable coronary plaques to sudden cardiac events. Lessons from a myocardial infarction-prone animal model (the WHHLMI rabbit) *J. Atheroscler. Thromb.* **11** 184–9
11. Whittaker P, Kloner R A, Boughner D R and Pickering J G 1994 Quantitative assessment of myocardial collagen with picrosirius red staining and circularly polarized light *Basic Res. Cardiol.* **89** 397–410
12. Pegoraro A F, Ridsdale A, Moffatt D J, Jia Y, Pezacki J P and Stolow A 2009 Optimally chirped multimodal CARS microscopy based on a single Ti:sapphire oscillator *Opt. Express* **17** 2984–96
13. K. Lang, J. Day, S. Eilerts, S. Fuqua, A. Guillen, M. Kordosky, M. Lang, J. Liu, W. Opaska, M. Proga, P. Vahle, A. Winbow, G. Drake, J. Thomas, C. Andreopoulos, N. Saoulidou, P. Stamoulis, G. Tzanakos, M. Zois, A. Weber, D. Michael 2005 Characterization of 1600 Hamamatsu 16-anode photomultipliers for the MINOS Far detector, *Nuclear Instruments and Methods in Physics*

Research Section A: Accelerators, Spectrometers, Detectors and Associated Equipment **545**, 852-871

14. N. Tagg, A. De Santo, A. Weber, A. Cabrera, P.S. Miyagawa, M.A. Barker, K. Lang, D. Michael, R. Saakyan, J. Thomas 2005 Performance of Hamamatsu 64-anode photomultipliers for use with wavelength--shifting optical fibres, *Nuclear Instruments and Methods in Physics Research Section A: Accelerators, Spectrometers, Detectors and Associated Equipment* **539**, 668-678
15. Yiping Shao, Robert W. Silverman, Simon R. Cherry 2000 Evaluation of Hamamatsu R5900 series PMTs for readout of high-resolution scintillator arrays, *Nuclear Instruments and Methods in Physics Research Section A: Accelerators, Spectrometers, Detectors and Associated Equipment* **454**, 379-388
16. Pologruto T A, Sabatini B L and Svoboda K 2003 ScanImage: flexible software for operating laser scanning microscopes *Biomed. Eng. Online* **2** 13
17. M. Strupler, A.-M. Pena, M. Hernest, P.-L. Tharaux, J.-L. Martin, E. Beaurepaire, and M.-C. Schanne-Klein 2007 Second harmonic imaging and scoring of collagen in fibrotic tissues, *Opt. Express* **15**, 4054-4065
18. Mostaço-Guidolin L B, Sowa M G, Ridsdale A, Pegoraro A F, Smith M D S, Hewko M D, Kohlenberg E K, Schattka B, Shiomi M, Stolow A and Ko A C-T 2010 Differentiating atherosclerotic plaque burden in arterial tissues using femtosecond CARS-based multimodal nonlinear optical imaging *Biomed. Opt. Express* **1** 59-73
19. Haralick R M, Shanmugam K and Dinstein I H 1973 Texture features for image classification *IEEE Trans. Sys. Man Cybernet.* **SMC-3** 610-21
20. Rasband, W S, 1997-2008ImageJ, *U. S. National Institutes of Health, Bethesda, Maryland*, USA, http://rsb.info.nih.gov/ij/
21. Pasterkamp G, Schoneveld A H, van der Wal A C, Haudenschild C C, Clarijs R J G, Becker A E, Hillen B and Borst C 1998 Relation of arterial geometry to luminal narrowing and histologic markers for plaque vulnerability: the remodeling paradox *J. Am. Coll. Cardiol.* **32** 655-62
22. Flueraru C, Kumazaki H, Sherif S, Chang S and Mao Y 2007 Quadrature Mach-Zehnder interferometer with application in optical coherence tomography *J. Opt. A: Pure Appl. Opt.* **9**, L5-8
23. Mao Y, Chang S, Sherif S and Flueraru C 2007 Graded-index fiber lens proposed for ultra-small probes used in biomedical imaging *Appl. Opt.* **46**, 5887-94
24. van der Meer F J, Faber D J, Perree J, Pasterkamp G, Baraznji Sassoon D, and van Leeuwen T G 2005 Quantitative optical coherence tomography of arterial wall components *IEEE Trans. Med. Imag.* **24** 1369-76
25. MacNeill B D, Lowe H C, Takano M, Fuster V, Jang I K 2002 Intravascular Modalities for Detection of Vulnerable Plaque *Atherosclerosis* **39** 604-9
26. van der Meer F J et al 2005 Quantitative optical coherence tomography of arterial wall components *Lasers Med. Sci.* **20** 45-51
27. Flueraru C, Popescu D P, Mao Y, Chang S and Sowa M G 2010 Added soft tissue contrast using the signal attenuation and the fractal dimension for optical coherence tomography images of porcine arterial tissue *Phys. Med. Biol.* **55** 2317-31
28. Popescu D P, Flueraru C, Mao Y, Chang S and Sowa M G 2010 Signal attenuation and box-counting fractal analysis of optical coherence images of arterial tissue *Biomed. Opt. Exp.* **1** 268-77
29. Le T T, Langohr I M, Locker M J, Sturek M and Cheng J X 2007 Label-free molecular imaging of atherosclerotic lesions using multimodal nonlinear optical microscopy *J. Biomed. Opt.* **12** 054007
30. Lilledahl M B, Haugen O A, de Lange Davies, C and Svaasand L O 2007 Characterization of vulnerable plaques by multiphoton microscopy *J. Biomed. Opt.* **12** 044005
31. Blankenhorn D H and Braunstein H 1958 Carotenoids in man. III. The microscopic pattern of fluorescence in atheromas, and its relation to their growth *J. Clin. Invest.* **37** 160–5

32. Arakawa K, Isoda K, Ito T, Nakajima K, Shibuya T and Ohsuzu F 2002 Fluorescence analysis of biochemical constituents identifies atherosclerotic plaque with a thin fibrous cap *Arterioscler. Thromb. Vasc. Biol.* **22** 1002–7
33. Motoyoshi I, Nishida S, Sharan L and Adelson E H 2007 Image statistics and the perception of surface qualities *Nature* **447** 206-9